online data

Sphingosine 1-phosphate analogue recognition and selectivity at $S1P_4$ within the endothelial differentiation gene family of receptors

Yuichi INAGAKI*[1], TrucChi T. PHAM†[1], Yuko FUJIWARA‡, Takayuki KOHNO*, Daniel A. OSBORNE†, Yasuyuki IGARASHI*, Gabor TIGYI†‡ and Abby L. PARRILL†‡[2]

*Department of Biomembrane and Biofunctional Chemistry, Graduate School of Pharmaceutical Sciences, Hokkaido University, Kita 12-jo, Nishi 6-choume, Kita-ku, Sapporo 060-0812, Japan, †Department of Chemistry and Computational Research on Materials Institute, The University of Memphis, Memphis, TN 38152, U.S.A., and ‡Department of Physiology, University of Tennessee Health Sciences Center, Memphis, TN 38163, U.S.A.

Synergistic computational and experimental studies provided previously unforeseen details concerning the structural basis of S1P (sphingosine 1-phosphate) recognition by the $S1P_4$ G-protein-coupled receptor. Similarly to reports on the $S1P_1$ receptor, cationic and anionic residues in the third transmembrane domain (R3.28 and E3.29 at positions 124 and 125) form ion pairs with the phosphate and ammonium of S1P, and alanine mutations at these positions abolished specific S1P binding, S1P-induced receptor activation and cell migration. Unlike findings on the $S1P_1$ receptor, no cationic residue in the seventh transmembrane domain interacts with the phosphate. Additionally, two previously undiscovered interactions with the S1P polar headgroup have been identified. Trp^{186} at position 4.64 in the fourth transmembrane domain interacts by a cation-π interaction with the ammonium group of S1P. Lys^{204} at position 5.38 forms an ion pair with the S1P. The $S1P_4$ and $S1P_1$ receptors show differences in binding-pocket shape and electrostatic distributions that correlate with the published structure–activity relationships. In particular, the binding pocket of $mS1P_4$ (mouse $S1P_4$) has recognition sites for the anionic phosphate and cationic ammonium groups that are equidistant from the end of the non-polar tail. In contrast, the binding pocket of $hS1P_1$ (human $S1P_4$) places the ammonium recognition site 2 Å (1 Å = 0.1 nm) closer to the end of the non-polar tail than the phosphate recognition site.

Key words: computational model, endothelial differentiation gene 6 (EDG6), G-protein-coupled receptor (GPCR), mutagenesis, sphingosine 1-phosphate (S1P), sphingosine 1-phosphate receptor 4 ($S1P_4$ receptor).

INTRODUCTION

S1P (sphingosine 1-phosphate) (Figure 1A) is a phospholipid mediator whose importance in immune function, cardiovascular development and cancer invasion is becoming increasingly evident [1–6]. S1P inhibits T-cell proliferation [7] and its endogenous presence in serum is required for optimal $CD4^+$ regulatory T-cell activity [8]. S1P elicits biological responses both through its action on GPCRs (G-protein-coupled receptors) embedded in the cell membrane as well as through activation of incompletely characterized intracellular targets [3,9–12].

The GPCRs responsive to S1P include five members of the endothelial differentiation gene (EDG) family: $S1P_1$/Edg1, $S1P_3$/Edg3, $S1P_2$/Edg5, $S1P_4$/Edg6 and $S1P_5$/Edg8, as well as another family of receptors, GPR3, GPR6 and GPR12 [6]. The $S1P_4$ receptor, with its restricted expression in the haematopoietic/immunopoietic cell lineage [13], shows approx. 60–200-fold reduced responsiveness to and affinity for S1P compared with other members of the EDG family [14,15]. Two natural S1P analogues, PHS1P (phytosphingosine 1-phosphate) [16,17] and DHS1P (dihydrosphingosine 1-phosphate) [17], have both been reported to bind $S1P_4$ with higher affinity than S1P. The 14-fold lower K_i of DHS1P than S1P at $S1P_4$ compared with the 8–10-fold lower concentration of DHS1P in serum from various species [18] suggests that DHS1P might be a biologically relevant agonist of $S1P_4$. $S1P_4$ activates calcium responses when overexpressed in CHO (Chinese-hamster ovary) cells through phospholipase C in a pertussis-toxin-sensitive fashion [19]. $S1P_4$ promotes cell migration [20,21], influences cell morphology [20] and may contribute to the fine balance of migration-stimulating [21–24] and migration-inhibiting [23,25,26] S1P receptors.

S1P recognition by select S1P receptors has been examined previously using agonist structure–activity relationships [14,27–31], computational modelling [31–35] and site-directed mutagenesis [33–35]. Integrated computational modelling and mutagenesis studies of the $S1P_1$ receptor have identified that charged residues in the third and seventh TMs (transmembrane domains) are crucial for S1P binding and S1P-induced receptor activation [33]. A residue in the third TM of $S1P_1$ and LPA_1 (lysophosphatidic acid receptor 1) serves as a selectivity switch for S1P against LPA recognition [35]. The present study examines recognition of S1P, PHS1P and DHS1P by the $S1P_4$ receptor, expanding on recognition of the polar headgroup of S1P and emphasizing differences in binding-pocket shape and electrostatic distribution that explain the preference of the $S1P_4$ receptor for saturated S1P analogues.

EXPERIMENTAL

Materials

S1P and PHS1P were purchased from Avanti Polar Lipids (Alabaster, AL, U.S.A.). Sphingosine was from Matreya (Pleasant Gap, PA, U.S.A.). Phytosphingosine and DHS1P were from

Abbreviations used: CHO, Chinese-hamster ovary; DHS1P, dihydrosphingosine 1-phosphate; EDG, endothelial differentiation gene; GPCR, G-protein-coupled receptor; [^{35}S]GTP[S], guanosine 5′-[γ-[^{35}S]thio]triphosphate; HA, haemagglutinin; HEK, human embryonic kidney; LPA, lysophosphatidic acid; MD, molecular dynamics; PHS1P, phytosphingosine 1-phosphate; RMSG, root mean square gradient; S1P, sphingosine 1-phosphate; (h)$S1P_1$, (human) S1P receptor 1; (m)$S1P_4$, (mouse) S1P receptor 4; TBST, Tris-buffered saline with Tween 20; TM, transmembrane domain; WT, wild-type.

[1] These authors contributed equally to this study.

[2] To whom correspondence should be addressed (email aparrill@memphis.edu).

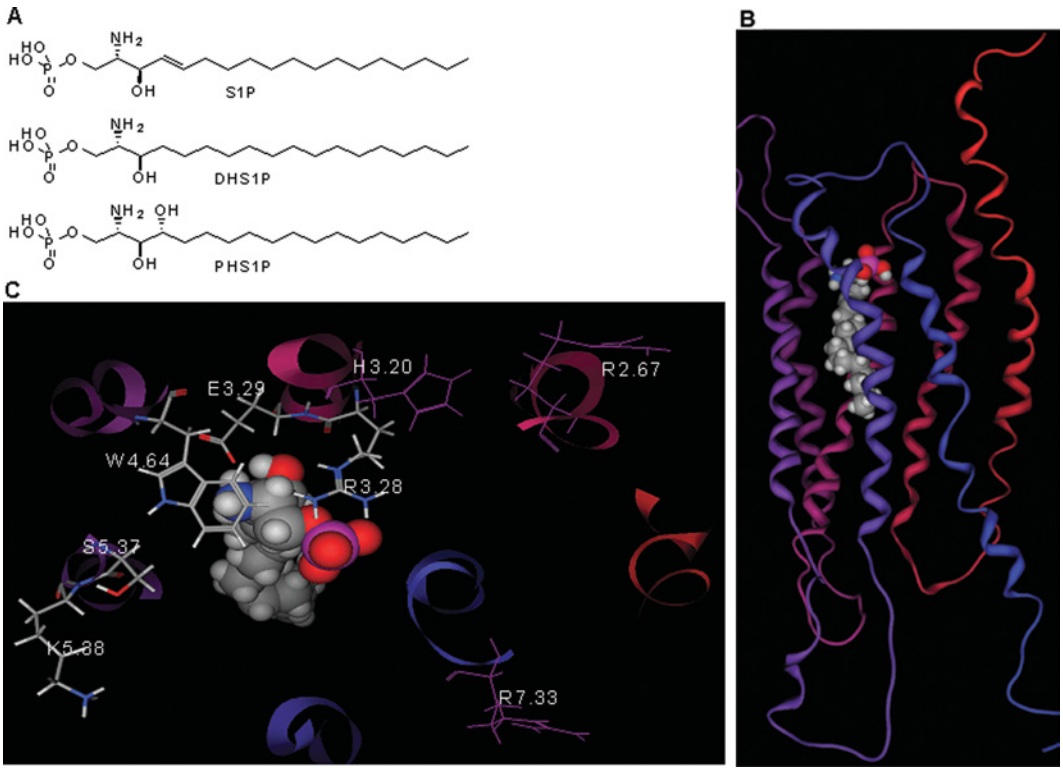

Figure 1 S1P, DHS1P, PHS1P and the S1P complex with mS1P$_4$

(**A**) Chemical structures of S1P, DHS1P and PHS1P. (**B**) The amino acid sequence of mS1P$_4$ was aligned against the hS1P$_1$ model, and a homology model was developed. The position of S1P was transferred from the hS1P$_1$ receptor model to the mS1P$_4$ receptor model. The model is shown with extracellular loops at the top. Ribbons coloured from red at the N-terminus to blue at the C-terminus represent the backbone of mS1P$_4$. The space-filling atoms represent S1P (red, oxygen; blue, nitrogen; grey, carbon; white, hydrogen; magenta, phosphorus). (**C**) View of the mS1P$_4$ complex with S1P from the extracellular space. Selected residues are shown as stick models and are labelled. Ribbons representing short segments of each TM are shown; the remainder are omitted for clarity. The colouring is as described for (**B**).

Biomol (Plymouth Meeting, PA, U.S.A.). BSA (fraction V), dihydrosphingosine and anti-γ-tubulin monoclonal antibody were from Sigma (St. Louis, MO, U.S.A.). Alexa Fluor® 488-conjugated goat anti-mouse IgG conjugate was from Molecular Probes (Eugene, OR, U.S.A.). Anti-FLAG M2 monoclonal antibody was from Stratagene (La Jolla, CA, U.S.A.) and anti-HA (haemagglutinin) antibody (Y-11) was purchased from Santa Cruz Biotechnology (Santa Cruz, CA, U.S.A.).

Development of an S1P$_1$-based homology model for mS1P$_4$ (mouse S1P$_4$)

The mS1P$_4$ model was developed based on the validated S1P$_1$ model [34] using the MOE software package from the Computational Chemistry Group (Montréal, Québec, Canada). The target sequence was aligned against the sequences of the EDG receptor family and bovine rhodopsin utilizing the MOE-Align facility. This function implements a modified version of the alignment methodology by Needleman and Wunsch [37]. Except for the target sequence and the template, all of the other sequences were removed before the mS1P$_4$ structure was generated by MOE-Homology. Owing to the lack of structural information for the N- and C- termini, the preliminary model included residues 33–328. The position of S1P was obtained by docking as described below. S1P was modelled with $+1$ ionization of the ammonium group and -1 ionization of the phosphate group.

Model optimization

In the present study, we employed both energy minimization and MD (molecular dynamics) to optimize the homology model of the mS1P$_4$ receptor. Both steps were performed with the MMFF94 force field [38]. Before the model was subjected to MD, we manually converted all *cis*-amide bonds into the *trans* conformation, with the exception of those at proline, and added S1P to the system by superimposition on the validated S1P$_1$ complex with S1P. The presence of the ligand prevents the binding pocket from collapsing during MD simulations. The mS1P$_4$ model was initially minimized for 1000 iterations of steepest descent, followed by conjugate gradient and Truncated Newton minimizations to a RMSG (root mean square gradient) of 0.01 kcal/mol · Å (1 cal $\equiv$ 4.184 J; 1 Å $=$ 0.1 nm). MD simulations were performed using a constant volume and temperature ensemble at an equilibrium temperature of 300 K using 1 fs time steps for 0.5 ns after a thermal equilibration period of 60 ps and dielectric constants of both 1 and 80. Snapshots were recorded every 1000 iterations for further structural evaluation. The minimized lowest energy complex from the dielectric constant of 1 ensemble was used to guide experimental mutagenesis. Mutation sites were selected from the model of the mS1P$_4$ complex with S1P either to validate apparent interactions between the receptor and agonist or as controls that were not expected to alter WT (wild-type) behaviour.

Experimentally driven model refinement

Discrepancies between model-based predictions and experimental observations clustered in TM5 necessitated revision of the hS1P$_1$ (human S1P$_1$) [33,35] and mS1P$_4$ models. New models of the S1P receptors were constructed using the alternative alignment of TM5, shown in Table 1. This alternative alignment was

Table 1 TM5 alignments used for homology model development

TM5 sequence alignment 1 was used for the development of the original $hS1P_1$-based bovine rhodopsin model [51] and the subsequent development of the $hS1P_1$-based $mS1P_4$ model. TM5 sequence alignment 2 was used for the experimentally driven refinement of the $hS1P_1$ and $mS1P_4$ models. Residues at position 5.50 are identified in bold. Numbering of S5.37 and K5.38 throughout are based on TM5 sequence alignment 2.

Receptor	TM5 sequence alignment 1	TM5 sequence alignment 2
Bovine rhodopsin	SFVIYMFVVHFII**P**LIVIFFCY	SFVIYMFVVHFII**P**LIVIFFCY
Human $S1P_1$	KHYILFCTTVFTL**L**LLSIVILY	HKHYILFCTTVFT**L**LLLSIVIL
Mouse $S1P_4$	KGYVLFCVVVFAL**I**LVAILSLY	SKGYVLFCVVVFA**L**ILVAILSL

used to generate models of human $S1P_1$ and subsequently $mS1P_4$. This model was optimized by geometry optimization and MD as described above. Additionally, the polar headgroups of S1P and nearby residues were partially solvated utilizing the solvation function on MOE. A total of 31 water molecules were included in the simulation, all starting within 11 Å of the polar headgroup of S1P. These waters were included to explore a possible indirect water-mediated interaction between S1P and neighbouring residues. The lowest energy structure from the MD simulation at a dielectric constant of 1 was minimized to generate refined $mS1P_4$ and $hS1P_1$ models which were used to generate mutant models and in docking studies with S1P.

Ligand docking

All docking studies were performed with Autodock version 3.0 [39]. This software allows exploration of ligand conformations, and configurations through torsion angle rotations, molecular translations and rotations in a rigid protein until an optimized site is found. Three Autodock parameters were modified from default values: (i) the number of energy evaluations in the genetic algorithm search was increased to 9×10^9, (ii) the optimization continued for 3×10^4 generations, and (iii) 3000 iterations were used in the local search. A docking box of $30.375 \times 24.375 \times 22.875$ Å^3 was used for docking S1P, PHS1P and DHS1P into $mS1P_4$ and $hS1P_1$. This box contained most of the transmembrane domains and all residues that were computationally and experimentally mutated to alanine.

DNA constructs

Construction and expression of the $mS1P_4$ plasmids was performed as described previously [21]. The $mS1P_4$ receptor was N-terminally tagged with the FLAG-epitope and C-terminally tagged with the HA-epitope and inserted into pcDNA3.1 vector (Invitrogen, Carlsbad, CA, U.S.A.).

Mutagenesis

Point mutations were introduced into pcDNA3-FLAG-$S1P_4$-HA as described previously [40]. PCR was performed using 0.4 ng of template DNA and mutagenic primers as follows (residues underlined represent the mutated codon): R2.67A (112) sense, 5′-ACTGCTACCTTCCAGCTGTCACCGGTG-3′ and R2.67A antisense, 5′-CCCTGACAGCAGCACGTTGACCACGTA-3′, H3.20A (120) sense, 5′-GTGGCTTGGTTCCTGCGGGAGGGCCTG-3′ and H3.20A antisense, 5′-CGGTGACAGCTGGAAGGTACGAGTCCC-3′, R3.28A sense, 5′-GAGGGCCTGCTCTTCATGGCCTTGGCC-3′ and R3.28A antisense, 5′-GGCCAGGAACCAGTGCACCGGTGACAG-3′, E3.29A sense, 5′-GCCGGCCTGCTCTTCATGGCCTTGGCC-3′ and E3.29A antisense, 5′-CCGCAGGAACCAGTGCACCGGTGACAG-3′, W4.64A sense, 5′-CTGCTGGGCGCCAACTGTGTGTGCGCC-3′ and W4.64A antisense, 5′-GGGCAGCAGGCCCAGGATAGCTGCCAG-3′, S5.37A sense, 5′-CCCCTCTACGCTAAGGGCTATGTGCTC-3′, K5.38A sense, 5′-CCCCTCTACTCCGCTGGCTATGTGCTC-3′, and S5.37A and K5.38A antisense, 5′-CAGCAGGCTGGAGCAGCGTGGGAAGGC-3′, and R7.33A sense, 5′-ATGGACTGGATCCTGGCCCTGGCCGTG-3′ and R7.33A antisense, 5′-GCCAGCCAGGTACTCCTGGGCCCAGAC-3′. The antisense primers were treated with T4 polynucleotide kinase (TaKaRa, Shiga, Japan). PCR was carried out in the presence of 0.2 mM dNTPs, 1 mM $MgCl_2$, 0.3 mM sense primer and polynucleotide-kinase-treated antisense primer for 30 cycles. The PCR products were ligated with the Ligation High kit (Toyobo, Tokyo, Japan). All mutations were confirmed by sequencing of the complete construct.

Cell culture and transfections

HEK-293T (human embryonic kidney) cells (A.T.C.C., Manassas, VA, U.S.A.) were grown in Dulbecco's modified minimum essential medium with high glucose supplemented with 10 % (v/v) foetal calf serum. CHO cells were cultured in Ham's F-12 medium (Sigma) containing 10 % (v/v) foetal calf serum, 100 units/ml penicillin and 10 μg/ml streptomycin. Cells were transfected using the Lipofectamine™ Plus kit (Invitrogen), according to the manufacturer's instructions. Stable clones expressing WT $mS1P_4$ and $mS1P_4$ mutants were selected in the presence of 600 μg/ml Geniticin (Sigma).

Western blot analysis

Cells were lysed with Laemmli sample buffer [62.5 mM Tris/HCl (pH 6.8), 2 % (w/v) SDS, 10 % (v/v) glycerol and 5 % (w/v) 2-mercaptoethanol]. The proteins were separated by SDS/PAGE and transferred on to a PVDF membrane (Millipore, Bedford, MA, U.S.A.). After blocking with 5 % (w/v) non-fat dried milk in TBST [Tris-buffered saline with Tween 20; 20 mM Tris/HCl (pH 7.5), 137 mM NaCl and 0.05 % (v/v) Tween 20], the blot was incubated with the anti-HA antibody, diluted 1:1000 in TBST, for 1 h at room temperature (25 °C). After four washes in TBST, the blot was incubated for 30 min at room temperature with horseradish-peroxidase-conjugated anti-rabbit IgG-$F(ab')_2$ fragment (Amersham Biosciences), diluted 1:10000 in TBST, and washed as above. Immunoreactive bands were visualized by the ECL® (enhanced chemiluminescence) plus detection kits (Amersham Biosciences).

Flow-cytometric analysis

Expression of $mS1P_4$ mutants at the cell surface was examined by flow cytometry using indirect immunofluorescence staining with anti-FLAG M2 monoclonal antibody. CHO cells were harvested by trypsinization and washed with ice-cold FACS buffer (PBS and 0.1 % BSA). After washing twice with FACS buffer, the cells were incubated at 4 °C for 60 min with the anti-FLAG M2 monoclonal antibody in FACS buffer (1:200 dilution). Subsequently, the cells were washed twice with FACS buffer, and then incubated with Alexa Fluor® 488-conjugated goat anti-mouse IgG secondary antibody (1:400 dilution) at 4 °C for 60 min. After washing the cells twice, samples were analysed using a FACSort flow cytometer (Beckton Dickinson, Palo Alto, CA, U.S.A.). Data were analysed with the Cell Quest software (Beckton Dickinson).

S1P, PHS1P and DHS1P radioligand binding assay

Preparation of radiolabelled ligands and binding assays were performed essentially as described previously [21]. Purified

MBP (maltose-binding protein)–mSPHK1 (murine sphingosine kinase 1) fusion protein was used for preparation of [^{32}P]S1P and [^{32}P]DHS1P. For preparation of [^{32}P]PHS1P, we used purified 3 × FLAG LCB4p. CHO cells (2×10^5) were incubated at 4 °C in binding buffer [20 mM Tris/HCl (pH 7.4), 100 mM NaCl, 15 mM NaF and 0.4 % (w/v) BSA] containing 60 nM (specific radioactivity 10 mCi/μmol) [^{32}P]S1P, [^{32}P]PHS1P or [^{32}P]DHS1P for 30 min. Non-specific binding was determined in the presence of 6 μM unlabelled competitor. Cells were washed three times with ice-cold binding buffer for 5 min and bound radioactivity was measured by liquid-scintillation counting.

S1P-activated [^{35}S]GTP[S] (guanosine 5′-[γ-[^{35}S]thio]triphosphate) binding assay

HEK-293T cells transiently transfected with the different receptor constructs were homogenized on day 2 in 20 mM Hepes (pH 7.5), 50 mM NaCl and 2 mM EDTA. Nuclei and cell debris were removed by centrifugation at 2000 ***g*** for 5 min at 4 °C, and the supernatant was centrifuged at 100 000 ***g*** for 1 h at 4 °C. The pellet containing the membrane fraction was rinsed with and then resuspended in 50 mM Hepes (pH 7.5), 100 mM NaCl, 1 mM $MgCl_2$ and 2 mM EDTA. A 10 μg sample of freshly prepared membrane protein was incubated in 100 μl of binding buffer containing 50 mM Hepes (pH 7.5), 100 mM NaCl, 5 mM $MgCl_2$, 10 μM GDP, 2 mM dithiothreitol, 50 μg/ml saponin, and 0.1 nM [^{35}S]GTP[S] (1000 Ci/mmol; Amersham Biosciences) and different concentrations of S1P for 30 min at 30 °C. Membrane-bound radioactivity was separated by filtration using a 96-well Brandel Cell Harvester (Gaithersburg, MD, U.S.A.) through a Whatman GF/B filter, rinsed with a total of 1 litre of 20 mM Tris/HCl (pH 7.4), 120 mM NaCl and 25 mM $MgCl_2$ wash buffer and quantified by liquid-scintillation counting. Samples were run in triplicate and their means ± S.D. were plotted as a function of S1P concentration.

Cell migration assay

The cell migration assay was performed as described previously [21]. Briefly, the number of cells migrating from the upper chamber to the lower surface of the Transwell filter (6.5 mm diameter, 8 μm pores; Corning Costar, Cambridge, MA, U.S.A.) was determined by counting the number of cells in five random fields.

Statistical methods

The significance of differences was determined by Student's *t* test. Values were considered significantly different at $P < 0.05$.

RESULTS

S1P$_1$-derived model of the mS1P$_4$ receptor

A model of the mS1P$_4$ receptor was developed by homology with our experimentally validated published hS1P$_1$ receptor model [33] with the TM5 alignment shown in Table 1. The mS1P$_4$ model was used in docking studies with S1P in order to identify amino acids with important roles in S1P recognition. The initial complex is shown in Figures 1(B) and 1(C). The model predicts, similar to S1P interactions with S1P$_1$, ion-pairing interactions between R3.28 (124) and the phosphate, as well as E3.29 (125) and the ammonium. W4.64 (186) makes a cation-π interaction with the ammonium of S1P, and interaction between the cationic residue in TM7, R7.33, and the phosphate is unclear. Three of the five S1P receptors have a cationic amino acid at position 7.34, which was demonstrated by mutagenesis to be required for S1P binding to and activation of S1P$_1$ [33]. The cationic residue in mS1P$_4$ differs by one position in the sequence alignment, and that in S1P$_5$ by more than a helical turn. Thus the importance of a cationic residue in TM7 of S1P$_1$ does not necessarily generalize to all S1P receptors. Although R7.33 faces away from the phosphate in the model, the side chain is flexible and sufficiently long to interact with the phosphate, given a less favourable side chain conformation. Thus this initial model leads to the hypothesis that mutations R3.28A, E3.29A and W4.64A would have a detrimental impact on S1P binding and activation. Additionally, mutations R2.67A (112A), H3.24A (120A), S5.37A (203A) and K5.38A (204A) would have little or no effect on binding and activation. The R7.33A (289A) mutation might have significant impact on binding.

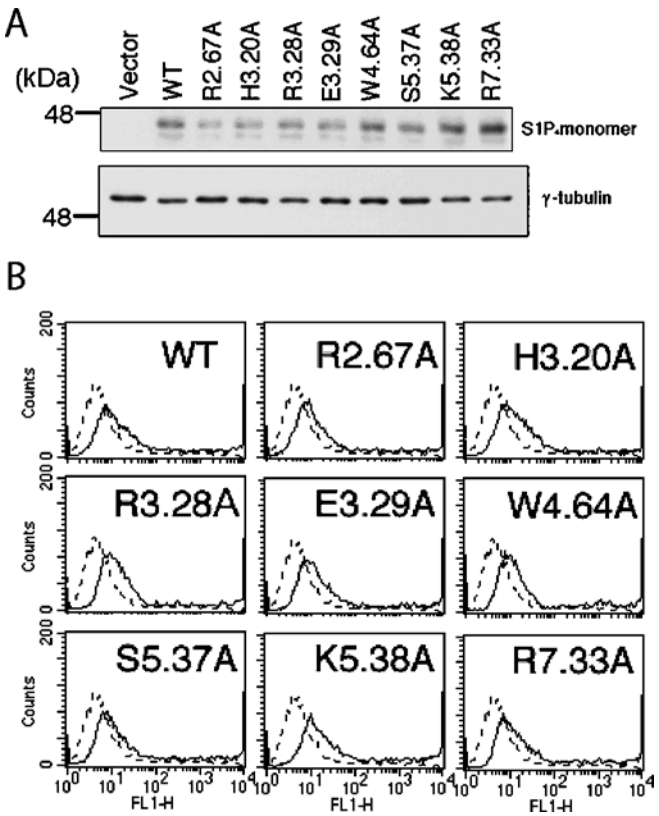

Figure 2 Expression of mS1P$_4$ and mS1P$_4$ mutants

(**A**) Expression of mS1P$_4$ and site-directed mutants was examined by Western blotting. CHO cells transfected with pcDNA3.1 empty vector, mS1P$_4$ or mS1P$_4$ mutants were detected by Western blotting with anti-HA antibody (upper panel). Anti-γ-tubulin blot from the same samples were performed as a control of sample loadings (lower panel). (**B**) Expression of mS1P$_4$ and site-directed mutants at the cell surface was examined by flow cytometry. CHO cells transfected with pcDNA3.1 empty vector, mS1P$_4$ or mS1P$_4$ mutants were detected with anti-FLAG M2 monoclonal antibody. Flow-cytometric analysis was performed as described in the Experimental section. The data are representative of three independent experiments. Broken lines indicate the signal obtained with vector-transfected control cells.

Expression and plasma membrane targeting of mS1P$_4$ mutants

Comparable levels of expression of epitope-tagged WT mS1P$_4$ and eight point mutants in CHO cells were evident from the intensity of the ~40 kDa band relative to γ-tubulin in the Western blot performed using membrane fractions of transiently transfected cells (Figure 2A). The FACS data shown in Figure 2(B) demonstrate comparable cell-surface localization of all constructs studied.

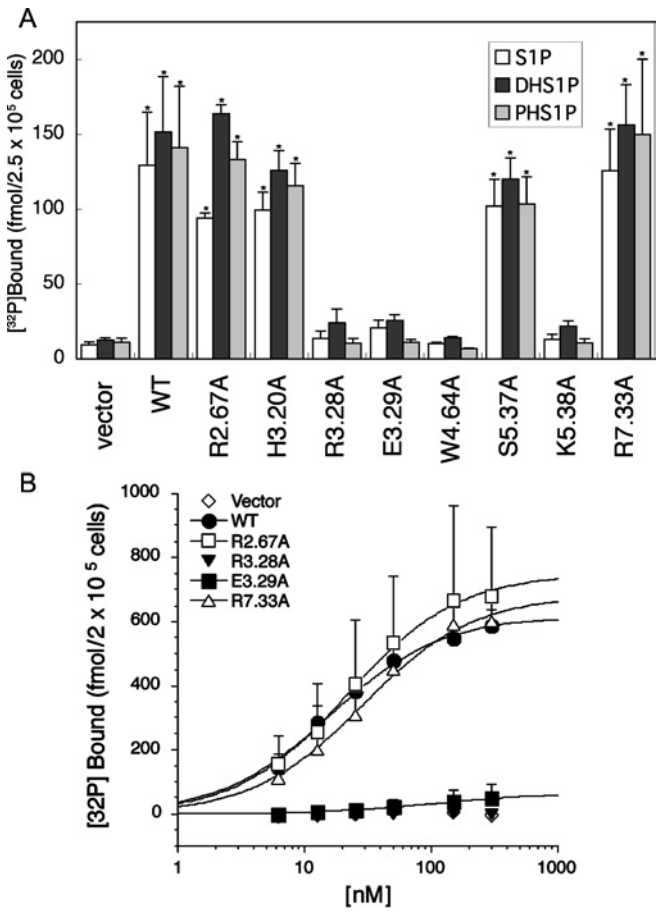

Figure 3 [^{32}P]S1P, [^{32}P]DHS1P and [^{32}P]PHS1P binding to mS1P$_4$ and mS1P$_4$ mutants

[^{32}P]S1P, [^{32}P]DHS1P and [^{32}P]PHS1P binding to WT mS1P$_4$ and mS1P$_4$ mutants. (**A**) CHO cells stably expressing empty vector, FLAG–S1P$_4$–HA or FLAG–S1P$_4$–HA mutants were incubated with 60 nM [^{32}P]S1P, [^{32}P]DHS1P or [^{32}P]PHS1P in the absence (total binding) or presence (non-specific binding) of 6 μM unlabelled competitor for 30 min at 4 °C. Cells were lysed, and bound radioligand was quantified by liquid-scintillation counting. Data show specific binding, which is binding in the absence of unlabelled competitor minus binding in the presence of 6 μM unlabelled competitor. Results are means $\pm$ S.E.M. for three independent experiments; $^*P < 0.05$ compared with vector control. (**B**) CHO cells stably expressing empty vector, FLAG–S1P$_4$–HA or FLAG–S1P$_4$–HA mutants were incubated with indicated concentrations of [^{32}P]S1P. Data show specific binding, which is binding in the absence of unlabelled competitor minus binding in the presence of unlabelled competitor. Results are means $\pm$ S.D. for three independent experiments.

Pharmacological characterization of mS1P$_4$ mutants

The roles of eight individual amino acids in the mS1P$_4$ receptor were tested experimentally using [^{32}P]S1P, [^{32}P]PHS1P and [^{32}P]DHS1P radioligand binding (Figure 3) and S1P-induced [^{35}S]GTP[S] binding assays (Figure 4). mS1P$_4$ or mutant mS1P$_4$ receptors were overexpressed in CHO and HEK-293 cells respectively for these assays. Northern blotting analysis demonstrated very low expression of only S1P$_2$ in CHO cells [41]. HEK-293 cells express S1P$_1$, S1P$_2$ and S1P$_3$ [42] at levels unlikely to be relevant in the presence of overexpressed constructs. As predicted by the model, the R3.28A, E3.29A and W4.64A mutations abolished specific S1P binding and S1P-induced receptor activation, thus confirming their importance for S1P binding and subsequent receptor activation. Control mutations R2.67A, H3.20A and S5.37A exhibited specific S1P binding comparable with WT, confirming that these positions do not interact with S1P.

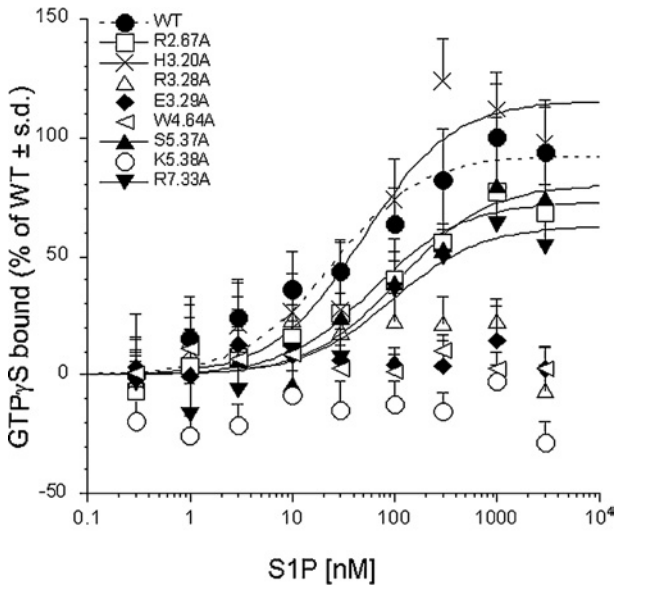

Figure 4 S1P-induced GTP[S] binding mediated by mS1P$_4$ and mS1P$_4$ mutants

Membranes prepared from HEK-293T cells transiently transfected with mS1P$_4$ or mS1P$_4$ mutants were incubated with 0.1 nM GTP[S] and different concentrations of S1P for 30 min at 30 °C. Membrane-bound radioactivity was separated by filtration and quantified by liquid-scintillation counting. Three independent experiments involving triplicate samples were performed. The means $\pm$ S.D. were plotted as a function of S1P concentration for a representative experiment. GTPγS, GTP[S].

Saturation binding analysis (Figure 3B) of R2.67A confirmed S1P binding potency similar to WT, with a K_d value ($\pm$S.D.) of 25.4 ($\pm$10.3) nM. S1P-induced receptor activation for these mutants, with EC_{50} values of 63, 49 and 110 nM for R2.67A, H3.20A and S5.37A was likewise comparable with WT, with an EC_{50} of 24 nM. The R7.33A mutant showed similar S1P binding to the WT receptor in these assays with a K_d value ($\pm$S.D.) of 33.6 ($\pm$19.4) nM, indicating that the side chain does not adopt the relatively high-energy conformation that would be necessary for it to interact with the phosphate group of S1P. The R7.33A mutant dose–response in the S1P-induced [^{35}S]GTP[S]-binding assay gave an EC_{50} of 94 nM, relative to the WT response of 24 nM. In contrast with the model-derived hypotheses, K5.38A failed to specifically bind S1P or activate in response to S1P. An indirect role of this residue is possible. However, the location of the residue in TM5, and the absence of the conserved proline residue found in TM5 of most GPCRs, suggests that the modelled positions of TM5 residues in the S1P$_1$-based mS1P$_4$ model might be incorrect.

mS1P$_4$ model refinement

Site-directed mutagenesis results revealed one discrepancy relative to the S1P$_1$-based mS1P$_4$ model. The inconsistency between the model and the experimental data occurs in TM5 of the mS1P$_4$ receptor, which lacks the conserved proline residue found in most GPCRs and which therefore had the least reliable alignment in the initial homology model development. The hS1P$_1$ and mS1P$_4$ models were refined by shifting each amino acid in the TM5 by one position as shown in Table 1. This effectively moves K5.38 of mS1P$_4$ to the position originally occupied by S5.37. The refined mS1P$_4$ model was optimized using MD with five layers of hydrating waters around the polar headgroup of S1P and the charged residues surrounding that headgroup, in order to explore potential

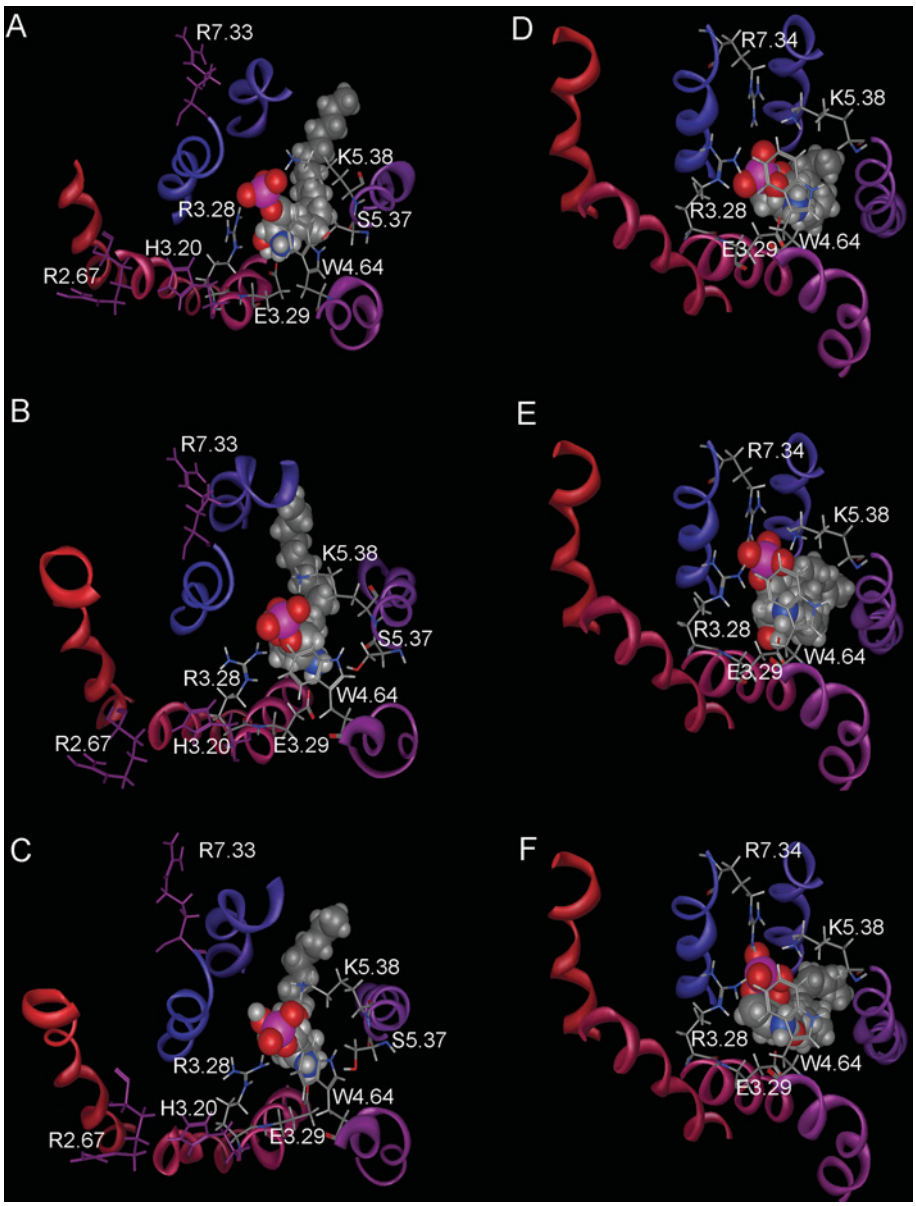

Figure 5 Refined WT mS1P$_4$ and hS1P$_1$ complexes with S1P, DHS1P and PHS1P

A refined mS1P$_4$ model was generated using the TM5 sequence alignment 2 from Table 1, which differs from the alignment initially used by one position only in TM5. A refined hS1P$_1$ model was generated in the same fashion. The models were generated using standard homology modelling methods in MOE followed by optimization by MD. Complexes with S1P, DHS1P and PHS1P generated by docking and refined by MD. Views of complexes are coloured as described for Figure 1(B) and include ribbons representing short segments of each TM, selected residues are labelled and shown as stick models and are shown from the extracellular space. (**A**) S1P$_4$ complex with S1P. (**B**) S1P$_4$ complex with DHS1P. (**C**) S1P$_4$ complex with PHS1P. (**D**) S1P$_1$ complex with S1P. (**E**) S1P$_1$ complex with DHS1P. (**F**) S1P$_1$ complex with PHS1P.

water-bridged interactions. The complex resulting from the hydrated molecular dynamics simulations is shown in Figure 5(A). No water-bridged interactions between mS1P$_4$ and S1P were observed. The refined model instead shows a clear ionic interaction between K5.38 and the phosphate group of S1P (Figure 5B). Thus the refined model is consistent with all experimental S1P binding and S1P-induced receptor activation results obtained with mS1P$_4$ and mS1P$_4$K5.38A.

S1P-induced cell migration

In order to evaluate whether the pharmacological impact of mutations was consistent with the cell-biological responses elicited by S1P-elicited activation, stably transfected cell lines expressing mS1P$_4$ and the eight mutants were characterized by assaying S1P-induced cell migration in a Transwell assay (Figure 6). S1P induced significant increases in cell migration when applied to cells expressing mS1P$_4$, R2.67A, H3.20A, S5.37A or R7.33A. In contrast, no increases in cell migration were observed in response to S1P application to R3.28A, E3.29A, W4.64A or K5.38A. These findings are consistent with the observed specific S1P binding and S1P-induced [^{35}S]GTP[S] binding for only the mS1P$_4$-, R2.67A-, H3.20A-, S5.37A- and R7.33A-expressing cells.

Ligand selectivity

The binding selectivities of mS1P$_4$ and mS1P$_1$ for S1P, PHS1P and DHS1P were determined using radioligand binding assays

on stably-transfected CHO cell lines. Supplementary Figure S1 (see http://www.BiochemJ.org/bj/389/bj3890187add.htm) shows dose–response curves for these sphingolipids binding to vector-, $mS1P_1$-, and $mS1P_4$-expressing cells. K_d values were obtained from these curves using curve-fitting analysis. K_d values ($\pm$S.D.) for $mS1P_1$ were 26.5 ($\pm$18.1), 36.0 ($\pm$20.4) and 38.4 ($\pm$29.5) nM for S1P, DHS1P and PHS1P, whereas K_d values ($\pm$S.D.) for $mS1P_4$ were 51.0 ($\pm$36.1), 37.2 ($\pm$21.7) and 51.0 ($\pm$19.2) nM respectively. The differences among these values do not even reach 2-fold, unlike the 10–20-fold DHS1P preference reported previously for $hS1P_4$ [17]. Three factors may contribute to the difference in the magnitude of ligand selectivity. First, Fossetta et al. [17] used K_i values obtained from competition binding experiments in contrast with our use of saturation binding analysis to derive K_d values. Secondly, the difference may be due to the reported difference in purity [17] between the DHS1P from Biomol used in these studies and that from Avanti used by Fossetta et al. [17]. Thirdly, the difference may reflect a species difference between the receptor sequences, which have 82 % residue identity. It has been observed previously for the adenosine A_1 receptor, another GPCR, that ligand selectivity preferences differ between species [43]. DHS1P and PHS1P binding to $mS1P_4$ mutants showed similar profiles as the binding of S1P to $mS1P_4$ mutants (Figure 3), suggesting a very similar bound orientation for the polar headgroups of the three lipids.

Computational complexes of $hS1P_1$ and $mS1P_4$ with S1P, DHS1P and PHS1P were generated by docking each lipid into the refined receptor models, followed by geometry optimization and MD simulations to allow relaxation of protein side chains in the vicinity of the bound ligands. Figure 5 demonstrates that these complexes display similar polar headgroup interactions. The phosphate groups of all three ligands form ion pairs with R3.28 and K5.38 in both receptors, and the ammonium groups of all three ligands form ion pairs with E3.29 and cation-π interactions with W4.64 in both receptors. Hydrogen bonds involving the single hydroxy group in S1P and DHS1P or the two hydroxy groups in PHS1P are observed to E3.29 in some structures sampled during the MD simulations, but occurred transiently and thus do not contribute strongly to the observed binding affinities.

DISCUSSION

The synergistic application of computational homology modelling and experimental site-directed mutagenesis has defined important features of S1P recognition in the $mS1P_4$ receptor. Some of these features are analogous to those identified previously in our previous studies on the $S1P_1$ receptor, namely the cationic residue R3.28, which ion pairs with the phosphate of S1P, and the anionic residue E3.29, which ion pairs with the ammonium group of S1P [33–35,44]. The present study also identifies two new conserved interactions. The first is between the cationic K5.38 residue and the phosphate of S1P in both $mS1P_4$ (Figure 5A) and $hS1P_1$ (Figure 5D). A second newly discovered interaction involves a cation-π interaction between the ammonium group of S1P and W4.64 in $mS1P_4$ (Figure 5A) and $hS1P_1$ (Figure 5D). One characteristic unique to the $mS1P_4$ receptor is the lack of interaction between a cationic residue in TM7 and the phosphate of S1P. These interactions were validated by experimental assay of S1P binding (Figure 3), S1P-induced [^{35}S]GTP[S] binding (Figure 4) and S1P-induced migration (Figure 6) in $S1P_4$-expressing cells, as well as S1P binding in $S1P_1$-transfected cells (see supplementary Figure S3 at http://www.BiochemJ.org/bj/389/bj3890187add.htm, and previous studies [33,35]). S1P responses in these assays were observed for cells or membranes from cells expressing $mS1P_4$, or its R2.67A, H3.20A, S5.37A and R7.33A, but not R3.28A, E3.29A, W4.64A and K5.38A mutants.

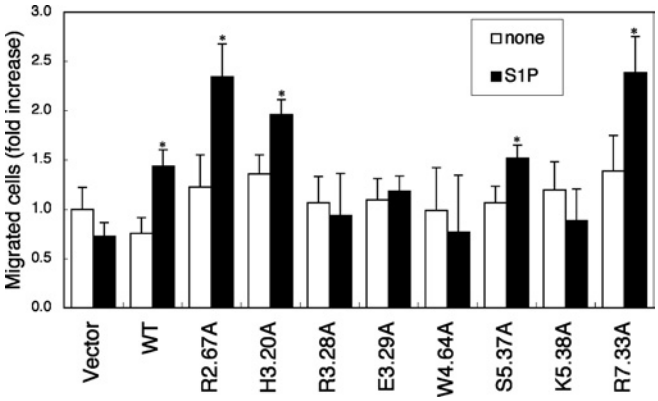

Figure 6 S1P-induced chemotaxis assay

CHO cells stably expressing empty vector, $mS1P_4$ or $mS1P_4$ mutants were tested in the cell migration assay as described under the Experimental section. Cells were added to the upper well of Transwell chambers, and 500 nM S1P was placed into the lower well. The number of vector-transfected cells transmigrating toward S1P-free medium (33 cells per field compared with 24 cells per field migrating toward S1P) was taken as a basal level. Results are means $\pm$ S.D. $^*P < 0.05$ compared with migration to S1P-free medium.

Models of both $S1P_1$ [31] and $S1P_4$ [32] have been published by other researchers. The $S1P_1$ model reported by Lim et al. [31] includes several features observed in our current models, as well as interactions that do not occur in our model. Consistent with our current model and our previous reports [33,35], Lim et al. [31] observe ion-pairing interactions between R3.28, R7.34 and the phosphate of S1P, as well as an ionic interaction between E3.29 and the ammonium group of S1P. The positions of W4.64 and K5.38 are not described. In contrast with our model, Lim et al. [31] suggest hydrogen bonds from the side chain hydroxy group of Y1.57 (98) and the backbone carbonyl group of F7.38 (296) to the hydroxy group of S1P. Figure 5(D) shows that, in our model, TM1 (red ribbon) is too distant from S1P for any residue to make direct contact with S1P. This difference between the models can be tested in future studies by site-directed mutagenesis. The $S1P_4$ model reported by Vaidehi et al. [32] shows very little similarity to our $mS1P_4$ model or our previously published $hS1P_4$ model [44]. Vaidehi et al. [32] note interactions between S1P and human $S1P_4$ residues T3.34 (127), E7.30 (284) and W7.37 (291), all displaced towards the extracellular loops compared with the residues mutated in the present study. The consistency between the $mS1P_4$-model-derived hypotheses and the experimental mutant characterization in the present study, as well as the observed receptor selectivity change to short-chain LPA species in the E3.29Q mutant [44], suggest that S1P is unlikely to interact with residues in the extracellular loops.

Tryptophan 4.64 is conserved in $S1P_{1–5}$, $LPA_{1–3}$ and the cannabinoid receptors, CB1 and CB2, although it is not found in other reported phospholipid receptors, GPR3/6/12 or LPA_4/P2Y9 [45]. Of these receptors, W4.64(172) mutations to alanine, leucine, phenylalanine and tyrosine have been reported for the CB2 receptor [46]. Mutations W4.64F and W4.64Y were found to retain binding to an aromatic, uncharged agonist. In contrast, mutations W4.64A and W4.64L resulted in loss of agonist binding. These results suggest that W4.64 is commonly located near the agonist-binding pocket in the EDG and cannabinoid families of lipid receptors, and can contribute to binding of either charged or aromatic agonists.

Relative affinities in the order DHS1P > PHS1P > S1P (Figure 1A) have been reported recently for human $S1P_4$, with a 10–20 fold preference for DHS1P based on K_i values determined from competition binding experiments [17]. Less than 2-fold differences were observed experimentally in the mouse $S1P_4$ and $S1P_1$ receptors studied here based on K_d values derived from saturation binding experiments (see supplementary Figure S1 at http://www.BiochemJ.org/bj/389/bj3890187add.htm). The relatively small differences in ligand preference observed may be due to the different experiments used to measure ligand binding, or to species differences between human and mouse $S1P_4$, which are only 82 % identical. Alternatively, they may be attributed to the use of DHS1P from Biomol, reported recently to be less potent than that from Avanti owing to purity [17]. Supporting the likelihood of experimental differences between the present study and that performed by Fossetta et al. [17] is the relatively similar K_d value of 63 nM obtained for S1P binding to $hS1P_4$ by Van Brocklyn et al. [47].

The shape difference of S1P in the $hS1P_1$ and $mS1P_4$ models is consistent with the known structure–activity relationships for $S1P_1$ and $S1P_4$. Yan et al. [48] reported recently a series of conformationally constrained piperidine- and pyrrolidine-containing phosphonic acids. Several *N*-alkyl 2-ethylphosphonic acids were tested, and all were unable to inhibit S1P binding to $S1P_4$, although several showed moderate inhibition of S1P binding to $S1P_1$. The reduced binding of such compounds relative to S1P at $S1P_1$ can be rationalized based on their non-linear geometry, which differs significantly from the geometry of S1P shown in supplementary Figure S2A (at http://www.BiochemJ.org/bj/389/bj3890187add.htm). However, they can still form all the important ion-pairing interactions and direct the alkyl chain into the hydrophobic binding channel owing to the disperse anionic surface that can accommodate a range of protonated nitrogen positions. In contrast, the very small region of anionic surface for interaction with a cationic nitrogen in $S1P_4$ (see supplementary Figure S2B at http://www.BiochemJ.org/bj/389/bj3890187add.htm) requires a very specific geometric relationship among the phosphate, ammonium and hydrophobic region for binding. The improved binding of the more extended 2-ethylphosphonic-3-alkyl piperidines at $S1P_1$ also supports the linear binding mode. In contrast with the selectivity observed for the conformationally restricted S1P analogues, the more flexible immunosuppressive phosphorylated form of FTY720 [49,50] shows binding to both $S1P_1$ and $S1P_4$ [15]. FTY720-phosphate can be described as a phosphorylated 2-alkyl-2-aminopropanediol, and thus can orient the phosphate, ammonium and alkyl chains in either a linear or bent shape to fit either the $S1P_1$ or $S1P_4$ binding pocket. The aromatic ring present in the hydrophobic chain of FTY720 begins at a position equivalent to carbon five of S1P, and thus would be in a position in the smaller hydrophobic channel of both $S1P_1$ and $S1P_4$ consistent with its high affinity for both receptors.

In conclusion, these findings identify S1P recognition features that generalize across the S1P receptor family as well as features unique to $S1P_4$. In particular, these studies highlight the previously unknown importance of cation-π interactions between W4.64 and the ammonium of S1P as well as ion-pairing interactions between the phosphate of S1P and K5.38 of both $S1P_4$ and $S1P_1$.

This work was supported in part by grants from NIH (National Institutes of Health) (1 RO1 CA92160-01), NSF-IBN9728147 and the American Heart Association (awards 0050006N and 0355199B). This work was supported in part by a Grant-in-aid for Scientific Research on Priority Area (B) 12140201 from the Ministry of Education, Culture, Sport, Science, and Technology, Japan. The Chemical Computing Group generously donated the MOE program. The purified 3 × FLAG LCB4p was kindly provided by Dr Iwaki and Dr Kihara (Igarashi Laboratory).

REFERENCES

1 Yamaguchi, H., Kitayama, J., Takuwa, N., Arikawa, K., Inoki, I., Takehara, K., Nagawa, H. and Takuwa, Y. (2003) Sphingosine-1-phosphate receptor subtype-specific positive and negative regulation of Rac and haematogenous metastasis of melanoma cells. Biochem. J. **374**, 715–722
2 Brinkmann, V., Davis, M. D., Heise, C. E., Albert, R., Cottens, S., Hof, R., Bruns, C., Prieschl, E., Baumruker, T., Hiestand, P. et al. (2002) The immune modulator, FTY720, targets sphingosine 1-phosphate receptors. J. Biol. Chem. **277**, 21453–21457
3 Hla, T. (2003) Signaling and biological actions of sphingosine 1-phosphate. Pharmacol. Res. **47**, 401–407
4 Matloubian, M., Lo, C. G., Cinamon, G., Lesneski, M. J., Xu, Y., Brinkmann, V., Allende, M. L., Proia, R. L. and Cyster, J. G. (2004) Lymphocyte egress from thymus and peripheral lymphoid organs is dependent on S1P receptor 1. Nature (London) **427**, 355–360
5 Osborne, N. and Stainier, D. Y. (2003) Lipid receptors in cardiovascular development. Annu. Rev. Physiol. **65**, 23–43
6 Parrill, A. L., Sardar, V. M. and Yuan, H. (2004) Sphingosine 1-phosphate and lysophosphatidic acid receptors: agonist and antagonist binding and progress toward development of receptor-specific ligands. Semin. Cell Dev. Biol. **15**, 467–476
7 Jin, Y., Knudsen, E., Wang, L., Bryceson, Y., Damaj, B., Gessani, S. and Maghazachi, A. A. (2003) Sphingosine 1-phosphate is a novel inhibitor of T-cell proliferation. Blood **101**, 4909–4915
8 Wang, W., Graeler, M. H. and Goetzl, E. J. (2004) Physiological sphingosine 1-phosphate requirement for optimal activity of mouse $CD4^+$ regulatory T cells. FASEB J. **18**, 1043–1045
9 Meyer zu Heringdorf, D., Liliom, K., Schaefer, M., Danneberg, K., Jaggar, J. H., Tigyi, G. and Jakobs, K. H. (2003) Photolysis of intracellular caged sphingosine-1-phosphate causes Ca^{2+} mobilization independently of G-protein-coupled receptors. FEBS Lett. **554**, 443–449
10 Spiegel, S. and Milstien, S. (2003) Exogenous and intracellularly generated sphingosine 1-phosphate can regulate cellular processes by divergent pathways. Biochem. Soc. Trans. **31**, 1216–1219
11 Van Brocklyn, J. R., Lee, M.-J., Menzeleev, R., Olivera, A., Edsall, L., Cuvillier, O., Thomas, D. M., Coopman, P. J. P., Thangada, S., Liu, C. H. et al. (1998) Dual actions of sphingosine-1-phosphate: extracellular through the G_i-coupled receptor Edg-1 and intracellular to regulate proliferation and survival. J. Cell Biol. **142**, 229–240
12 Ignatov, A., Lintzel, J., Kreienkamp, H. and Schaller, H. C. (2003) Sphingosine-1-phosphate is a high-affinity ligand for the G protein-coupled receptor GPR6 from mouse and induces intracellular Ca^{2+} release by activating the sphingosine-kinase pathway. Biochem. Biophys. Res. Commun. **311**, 329–336
13 Gräler, M. H., Bernhardt, G. and Lipp, M. (1998) EDG6, a novel G-protein-coupled receptor related to receptors for bioactive lysophospholipids, is specifically expressed in lymphoid tissue. Genomics **53**, 164–169
14 Clemens, J. J., Davis, M. D., Lynch, K. R. and Macdonald, T. L. (2003) Synthesis of *para*-alkyl aryl amide analogues of sphingosine-1-phosphate: discovery of potent S1P receptor agonists. Bioorg. Med. Chem. Lett. **13**, 3401–3404
15 Mandala, S., Hajdu, R., Bergstrom, J., Quackenbush, E., Xie, J., Milligan, J., Thornton, R., Shei, G., Card, D., Keohane, C. et al. (2002) Alteration of lymphocyte trafficking by sphingosine 1-phosphate receptor agonists. Science **296**, 346–349
16 Rios Candelore, M., Wright, M. J., Tota, L. M., Milligan, J., Shei, G., Bergstrom, J. D. and Mandala, S. M. (2002) Phytosphingosine 1-phosphate: a high affinity ligand for the S1P4/Edg-6 receptor. Biochem. Biophys. Res. Commun. **297**, 600–606
17 Fossetta, J., Deno, G., Gonsiorek, W., Fan, X., Lavey, B., Das, P., Lunn, C., Zavodny, P. J., Lundell, D. and Hipkin, R. W. (2004) Pharmacological characterization of human S1P4 using a novel radioligand, [4,5-^{3}H]-dihydrosphingosine-1-phosphate. Br. J. Pharmacol. **142**, 851–860
18 Min, J. K., Yoo, H. S., Lee, E. Y., Lee, W. J. and Lee, Y. M. (2002) Simultaneous quantitative analysis of sphingoid base 1-phosphates in biological samples by o-phthalaldehyde precolumn derivatization after dephosphorylation with alkaline phosphatase. Anal. Biochem. **303**, 167–175
19 Yamazaki, Y., Kon, J., Sato, K., Tomura, H., Sato, M., Yoneya, T., Okazaki, H., Okajima, F. and Ohta, H. (2000) Edg-6 as a putative sphingosine 1-phosphate receptor coupling to Ca^{2+} signaling pathway. Biochem. Biophys. Res. Commun. **268**, 583–589
20 Gräler, M. H., Grosse, R., Kusch, A., Kremmer, E., Gudermann, T. and Lipp, M. (2003) The sphingosine 1-phosphate receptor S1P4 regulates cell shape and motility via coupling to G_i and $G_{12/13}$. J. Cell. Biochem. **89**, 507–519
21 Kohno, T., Matsuyuki, H., Inagaki, Y. and Igarashi, Y. (2003) Sphingosine 1-phosphate promotes cell migration through the activation of Cdc42 in Edg-6/S1P4-expressing cells. Genes Cells **8**, 685–697
22 Osada, M., Yatomi, Y., Ohmori, T., Ikeda, H. and Ozaki, Y. (2002) Enhancement of sphingosine 1-phosphate-induced migration of vascular endothelial cells and smooth muscle cells by an EDG-5 antagonist. Biochem. Biophys. Res. Commun. **299**, 483–487

23 Dolezalova, H., Shankar, G., Huang, M., Bikle, D. D. and Goetzl, E. J. (2003) Biochemical regulation of breast cancer cell expression of S1P2 (Edg-5) and S1P3 (Edg-3) G protein-coupled receptors for sphingosine 1-phosphate. J. Cell. Biochem. **88**, 732–743

24 Takuwa, Y. (2002) Subtype-specific differential regulation of Rho family G proteins and cell migration by the Edg family sphingosine-1-phosphate receptors. Biochim. Biophys. Acta **1582**, 112–120

25 Ryu, Y., Takuwa, N., Sugimoto, N., Sakurada, S., Usui, S., Okamoto, H., Matsui, O. and Takuwa, Y. (2002) Sphingosine-1-phosphate, a platelet-derived lysophospholipid mediator, negatively regulates cellular Rac activity and cell migration in vascular smooth muscle cells. Circ. Res. **90**, 325–332

26 Arikawa, K., Takuwa, N., Yamaguchi, H., Sugimoto, N., Kitayama, J., Nagawa, H., Takehara, K. and Takuwa, Y. (2003) Ligand-dependent inhibition of B16 melanoma cell migration and invasion via endogenous S1P2 G protein-coupled receptor: requirement of inhibition of cellular RAC activity. J. Biol. Chem. **278**, 32841–32851

27 Lim, H., Oh, Y., Suh, P. and Chung, S. (2003) Syntheses of sphingosine-1-phosphate stereoisomers and analogues and their interaction with EDG receptors. Bioorg. Med. Chem. Lett. **13**, 237–240

28 Lu, X., Cseh, S., Byun, H. S., Tigyi, G. and Bittman, R. (2003) Total synthesis of two photoactivatable analogues of the growth-factor-like mediator sphingosine 1-phosphate: differential interaction with protein targets. J. Org. Chem. **68**, 7046–7050

29 Hakogi, T., Shigenari, T., Katsumura, S., Sano, T., Kohno, T. and Igarashi, Y. (2003) Synthesis of fluorescence-labeled sphingosine and sphingosine 1-phosphate: effective tools for sphingosine and sphingosine 1-phosphate behavior. Bioorg. Med. Chem. Lett. **13**, 661–664

30 Im, D.-S., Clemens, J., Macdonald, T. L. and Lynch, K. R. (2001) Characterization of the human and mouse sphingosine 1-phosphate receptor, S1P5 (Edg-8): structure–activity relationship of sphingosine 1-phosphate receptors. Biochemistry **40**, 14053–14060

31 Lim, H., Park, J., Ko, K., Lee, M. and Chung, S. (2004) Syntheses of sphingosine-1-phosphate analogues and their interaction with EDG/S1P receptors. Bioorg. Med. Chem. Lett. **14**, 2499–2503

32 Vaidehi, N., Floriano, W. B., Trabanino, R., Hall, S. E., Freddolino, P., Choi, E. J., Zamanakos, G. and Goddard, W. A. I. (2002) Prediction of structure and function of G protein-coupled receptors. Proc. Natl. Acad. Sci. U.S.A. **99**, 12622–12627

33 Parrill, A. L., Wang, D.-A., Bautista, D. L., Van Brocklyn, J. R., Lorincz, Z., Fischer, D. J., Baker, D. L., Liliom, K., Spiegel, S. and Tigyi, G. (2000) Identification of Edg1 receptor residues that recognize sphingosine 1-phosphate. J. Biol. Chem. **275**, 39379–39384

34 Parrill, A. L., Baker, D. L., Wang, D., Fischer, D. J., Bautista, D. L., van Brocklyn, J., Spiegel, S. and Tigyi, G. (2000) Structural features of EDG1 receptor–ligand complexes revealed by computational modeling and mutagenesis. In Lysophospholipids and Eicosanoids in Biology and Pathophysiology, vol. 905 (Goetzl, E. J. and Lynch, K. R., eds.), pp. 330–339, New York Academy of Sciences, New York

35 Wang, D., Lorincz, Z., Bautista, D. L., Liliom, K., Tigyi, G. and Parrill, A. L. (2001) A single amino acid determines ligand specificity of the $S1P_1$ (EDG1) and LPA_1 (EDG2) phospholipid growth factor receptors. J. Biol. Chem. **276**, 49213–49220

36 Reference deleted

37 Needleman, S. B. and Wunsch, C. D. (1970) A general method applicable to the search for similarities in the amino acid sequence of two proteins. J. Mol. Biol. **48**, 443–453

38 Halgren, T. A. (1996) Merck Molecular Force Field. I. basis, form, scope, parameterization, and performance of MMFF94*. J. Comput. Chem. **17**, 490–519

39 Morris, G. M., Goodsell, D. S., Halliday, R. S., Huey, R., Hart, W. E., Belew, R. K. and Olson, A. J. (1998) Automated docking using a Lamarckian genetic algorithm and an empirical binding free energy function. J. Comput. Chem. **19**, 1639–1662

40 Kohno, T., Wada, A. and Igarashi, Y. (2002) N-Glycans of sphingosine 1-phosphate receptor Edg-1 regulate ligand-induced receptor internalization. FASEB J. **16**, 983–992

41 Okamoto, H., Takuwa, N., Gonda, K., Okazaki, H., Chang, K., Yatomi, Y., Shigematsu, H. and Takuwa, Y. (1998) EDG1 is a functional sphingosine-1-phosphate receptor that is linked via a $G_{i/o}$ to multiple signaling pathways, including phospholipase C activation, Ca^{2+} mobilization, Ras-mitogen-activated protein kinase activation, and adenylate cyclase inhibition. J. Biol. Chem. **273**, 27104–27110

42 Meyer zu Heringdorf, D., Lass, H., Kuchar, I., Lipinski, M., Alemany, R., Rumenapp, U. and Jakobs, K. H. (2001) Stimulation of intracellular sphingosine-1-phosphate production by G-protein-coupled sphingosine-1-phosphate receptors. Eur. J. Pharmacol. **414**, 145–154

43 Tucker, A. L., Robeva, A. S., Taylor, H. E., Holeton, D., Backner, M., Lynch, K. R. and Linden, J. (1994) A_1 adenosine receptors: two amino acids are responsible for species differences in ligand recognition. J. Biol. Chem. **269**, 27900–27906

44 Holdsworth, G., Osborne, D. A., Pham, T. T., Fells, J. I., Hutchinson, G., Milligan, G. and Parrill, A. L. (2004) A single amino acid determines preference between phospholipids and reveals length restriction for activation of the S1P4 receptor. BMC Biochem. **5**, 12

45 Horn, F., Vriend, G. and Cohen, F. E. (2001) Collecting and harvesting biological data: the GPCRDB and NucleaRDB information systems. Nucleic Acids Res. **29**, 346–349

46 Rhee, M.-H., Nevo, I., Bayewitch, M. L., Zagoory, O. and Vogel, Z. (2000) Functional role of tryptophan residues in the fourth transmembrane domain of the CB2 cannabinoid receptor. J. Neurochem. **75**, 2485–2491

47 Van Brocklyn, J. R., Gräler, M. H., Bernhardt, G., Hobson, J. P. and Spiegel, S. (2000) Sphingosine-1-phosphate is a ligand for the G protein-coupled receptor EDG-6. Blood **95**, 2624–2629

48 Yan, L., Hale, J. J., Lynch, C. L., Budhu, R., Gentry, A., Mills, S. G., Hajdu, R., Keohane, C. A., Rosenbach, M. J., Milligan, J. A. et al. (2004) Design and synthesis of conformationally constrained 3-(*N*-alkylamino)propylphosphonic acids as potent agonists of sphingosine-1-phosphate (S1P) receptors. Bioorg. Med. Chem. Lett. **14**, 4861–4866

49 Brinkmann, V. and Lynch, K. R. (2002) FTY720: targeting G-protein-coupled receptors for sphingosine 1-phosphate in transplantation and autoimmunity. Curr. Opin. Immunol. **14**, 569–575

50 Chiba, K., Yanagawa, Y., Masubuchi, Y., Kataoka, H., Kawaguchi, T., Ohtsuki, M. and Hoshino, Y. (1998) FTY720, a novel immunosuppressent, induces sequestration of circulating mature lymphocytes by acceleration of lymphocyte homing in rats. I. FTY720 selectively decreases the number of circulating mature lymphocytes by acceleration of lymphocyte homing. J. Immunol. **160**, 5037–5044

51 Pogozheva, I. D., Lomize, A. L. and Mosberg, H. I. (1997) The transmembrane 7-a-bundle of rhodopsin: distance geometry calculations with hydrogen bonding constraints. Biophys. J. **70**, 1963–1985

Received 5 January 2005/21 February 2005; accepted 25 February 2005
Published as BJ Immediate Publication 25 February 2005, DOI 10.1042/BJ20050046